ORIGINAL SCIENTIFIC PAPER

CROATICA CHEMICA ACTA

Croat. Chem. Acta **2017**, *90*(2), 289–295
Published online: August 29, 2017
DOI: 10.5562/cca3180

HKD 1926

Electrochemical Characterisation of Sol-Gel Derived SnO_2 for Supercapacitor Application

Marijana Kraljić Roković,[1,*] Gabrijela Ljubek,[2] Mark Žic,[3] Jasminka Popović[3]

[1] Faculty of Chemical Engineering and Technology, University of Zagreb, Marulićev trg 19, HR-10000 Zagreb, Croatia
[2] Faculty of Mining, Geology and Petroleum Engineering, University of Zagreb, Pierottijeva 6, HR-10000 Zagreb, Croatia
[3] Ruđer Bošković Institute, Bijenička cesta 54, HR-10000 Zagreb, Croatia
* Corresponding author's e-mail address: mkralj@fkit.hr

RECEIVED: June 2, 2017 * REVISED: July 19, 2017 * ACCEPTED: July 23, 2017

THIS PAPER IS DEDICATED TO PROF. MIRJANA METIKOŠ-HUKOVIĆ ON THE OCCASION OF HER BIRTHDAY

Abstract: Pseudocapacitive properties of SnO_2 and Sb-doped SnO_2 were determined in 0.5 mol dm^{-3} KCl solution. The samples were prepared by sol-gel method and analysed by X-ray powder diffraction (XRPD) and field emission scanning electron microscopy (FE SEM). Rietveld refinement of XRPD data showed the changes in unit cell parameters due to the incorporation of Sb^{3+} into the host SnO_2 lattice, while FE SEM pointed out the differences in morphology caused by doping. Specific capacitance values of 3.67 and 6.89 F g^{-1} were obtained for SnO_2 and Sb-doped SnO_2, respectively. Reaction mechanism of SnO_2 that corresponds to the obtained mass change was proposed. It was shown that redox reactions of SnO_2 and Sb-doped SnO_2 are dependent on structural changes since different mass change properties were obtained in comparison to the previous reports carried out for other metal oxides.

Keywords: SnO_2, Sb-doped SnO_2, supercapacitors, cyclic voltammetry, electrochemical quartz crystal nanobalance.

INTRODUCTION

In recent years, a great deal of attention has been paid to supercapacitors due to high power density that can be achieved. Their development is focused on active materials that are required to provide both high power and high energy density. Commercially available supercapacitors mostly contain carbon as active material and their capacitive mechanism is based on double layer charging / discharging. Specific capacitance values of these materials are limited to 200 F g^{-1} and governed by carbon specific surface area and electrolyte accessibility to the highly developed surface. Therefore, in order to achieve higher specific capacitance, different materials, such as metal oxides and conductive polymers, have been investigated.[1–3] These materials have different charge storage mechanism that includes reversibile redox reaction with pseudocapacitive response. It is well known that RuO_2 has outstanding pseudocapacitive properties with high specific capacitance values that goes up to 720 F g^{-1}.[4] However, RuO_2 is expensive and rather rare oxide and for that reason there are continuous attempts to replace it with cheaper metal oxides such as MnO_2, Fe_2O_3, Co_3O_4, V_2O_5 and SnO_2, as well as with metal oxide composites containing carbon, carbon nanotube or graphene.[2,5,8,9] Hence, it is important for these materials to meet requirements related to abundance and environmental safety.

SnO_2 possesses unique optical and electrical properties that enables its application in catalysis, gas sensors, solar cells and transparent electrode materials. Tin-based materials attract also a considerable attention as an electrode material for other energy storage applications.[10–19] SnO_2 has been used as anode material for Li secondary batteries,[10,11] but its pseudocapacitive properties were also studied.[12–19] In order to overcome the problems addressed to SnO_2, such as electrical conductivity and structural stability of SnO_2, it is very often prepared in the presence of graphene,[5,8] carbon,[9,11,13,16,18,19] other metal oxides[12,15] or with a hollow structure.[10]

J. Liu *et al.*[12] have successfully fabricated pristine Fe_3O_4 / SnO_2 core / shell nanorods on Ti-substrate and

investigated their electrochemical performance for energy storage. The nanorods have shown good cycling stability of up to 2000 charging / discharging cycles and displayed high capacitance promising in thin-film supercapacitors. It has been concluded that the charge storage includes redox reactions of SnO_2 followed by intercalation of the electrolyte cations (Na^+) into the SnO_2 structure.

S. Ren *et al.*[13] showed that carbon-coated SnO_2 hollow spheres have good capacitive properties with capacitance values ranging from 30–45 F g^{-1}. Y.S. Lee *et al.*[14] studied SnO_2 and Co-doped SnO_2 nanoparticle obtained by hydrothermal method. The obtained product showed good pseudocapacitive properties within potential range from –0.8 to –0.1 V in 1 mol dm^{-3} H_2SO_4 and specific capacitance values up to 840 F g^{-1} at 10 mV s^{-1}. V. Velmurugan *et al.*[8] have shown that overall specific capacitance of SnO_2/graphene composite electrodes corresponds to the combined contribution from electrochemical double layer charging and pseudocapacitive behaviour of the composite. The resultant specific capacitance was 50 F g^{-1} in the case of pure SnO_2 and 100 F g^{-1} for SnO_2 / graphene composite at the scan rate of 50 mV s^{-1}. At low scan rates the authors have obtained much higher values of specific capacitance, 470 and 818 F g^{-1} for the same electrode. However, supercapacitors should have high capacitance at much higher charge / discharge rates and therefore low scan rates are not relevant for its characterisation. From the previous investigations,[12–19] it is evident that specific capacitance value of SnO_2 can vary significantly, depending on the method of preparation. Since SnO_2 was investigated in various potential ranges, it is not completely clear in which potential range SnO_2 pseudocapacitive properties should be optimally utilized.

The aim of this work was to determine a potential range at which the most of SnO_2 pseudocapacitive properties can be optimally utilised and to propose the reaction mechanism responsible for SnO_2 pseudocapacitive response in neutral aqueous electrolyte solutions. In the previous investigations, mostly composite materials containing SnO_2 were investigated wherein both double layer charging and pseudocapacitance contributed to overall capacitance. Although better capacitive properties have been reported for composite materials, additional investigations of pure SnO_2 are required to clarify its pseudocapacitive behaviour. In order to improve the SnO_2 performances, Sb-doped SnO_2 was also investigated in this work. The pure and Sb-doped SnO_2 were successfully synthesized *via* simple wet chemical process (*i.e.*, sol-gel method). The prepared materials were characterized by means of cyclic voltammetry, quartz crystal nanobalance (EQCN), X-Ray powder diffraction (XRPD) and field emission scanning electron microscopy (FE SEM).

EXPERIMENTAL

SnO_2 was prepared by the sol-gel method as follows. In a typical synthesis, $SnCl_2$ (Acros Organics) was dissolved in 10 mL of absolute ethanol (Gram-Mol) to prepare 0.3 mol dm^{-3} solution. The solution was added drop-wise to 50 mL of 9 : 1 ethanol / water mixture and consequently colloid suspension was obtained. Gelous precipitate, obtained from colloidal suspension, was washed several times with water in order to remove Cl^-. Washed precipitate was dried at 120 °C, during 1 h and afterwards heated at 500 °C during 2 h in air. In order to prepare Sb-doped SnO_2, the absolute ethanol solution of 0.3 mol dm^{-3} $SnCl_2$ was added to 0.03 mol dm^{-3} absolute ethanol solution of $SbCl_3$ (Lach-Ner). Both solutions were mixed in the ratio that gives the final Sn:Sb mole ratio of 1 : 0.03. Obtained solution was exposed to ultrasonic agitation for 15 min and added drop-wise to the mixture of 50 mL of 9 : 1 ethanol / water. The same washing, drying and heating procedures were carried out as in the case of pure SnO_2 preparation.

To prepare electrodes, the obtained SnO_2 and Sb-doped SnO_2 powders were mixed with paraffin oil (Fluka) and the resulting slurry was spread onto a glassy carbon support. The electrode layers were finally formed by heating at 450 °C for 45 min. The geometric electrode area was 0.15 cm^2 and the mass of layers were 5 mg.

For the electrochemical quartz crystal nanobalance (EQCN) measurements, the frequency of the quartz crystal coated with platinum was monitored by SEIKO EG&G QCA 917 quartz crystal nano-balance connected to the potentiostat. The fundamental frequency was 9 MHz and the integral sensitivity was 8.19×10^{-7} Hz cm^2 g^{-1}. The working area of an electrode and piezoelectrically active area were 0.2 cm^2. The mass of material applied on an EQCN platinum support was approximately 50 μg. The electrode was prepared by the same procedure as to apply SnO_2 and Sb-doped SnO_2 on glassy carbon support.

Cyclic voltammetry experiments were conducted in an one-compartment three-electrode electrochemical cell by means of Potentiostat/Galvanostat PAR, model 263A. Pt-foil served as counter-electrode (0.5 cm^2), and saturated calomel electrode (SCE) as the reference electrode. All potentials in this work are referred to SCE. SnO_2-based layers were tested by cyclic voltammetry and the EQCN method in the potential region from –0.5 to 0.8 V in 0.5 mol dm^{-3} KCl solution at scan rates of 10–300 mV s^{-1}. The experiments were carried out at room temperature (t = 23 ± 2 °C). A solution of 0.5 mol dm^{-3} KCl was prepared by using bi-distilled water and KCl (Kemika, p.a.).

Structural characterization was performed by the X-ray powder diffraction (XRPD) at room temperature using a Philips MPD 1880 counter diffractometer with monochromatized CuKα radiation. Data was collected in the 2θ range

from 20 to 80°, with a fixed counting time of 2 s per step. Rietveld refinement on XRPD data was performed in HighScoreXpert 4.5 program using the pseudo-Voigt profile function and the polynomial background model. Six background parameters, zero-point shift, mixing parameter (describing contributions of Gaussian and Lorentzian profile to the total line profile), line width parameters (*U*, *V*, *W*), and asymmetry parameter were included in the refinement together with the structural parameters. Silicon powder (99.999 %, Koch-Light Lab Ltd., UK) was used as a standard for instrumental diffraction-line broadening. Uncertainty values associated with XDR parameters are given in brackets and they represent the mean error that is equal to square root of variance.

FE SEM images were obtained on JSM-7000F thermal field emission scanning electron microscope manufactured by Jeol Ltd. FE SEM was coupled with EDS/INCA 350 (energy dispersive X-ray analyser) manufactured by Oxford Instruments Ltd. The samples were not coated with a conductive layer.

Thermal analysis was performed using thermo-gravimetric analyzer TA instrument Q 500. The water content of the material was estimated from the amount of weight loss in temperature range from 25 °C up to 700 °C assuming that SnO_2 at 700 °C is completely anhydrous. Samples were heated at rate 10 °C min^{-1} in air gas flow of 40 mL min^{-1}. Physisorbed water was estimated from weight loss up to 100 °C while chemisorbed water was estimated from weight loss at temperatures above 200 °C.

RESULTS AND DISCUSSION

Figure 1 shows Rietveld refinements for pure and Sb-doped SnO_2 powders, which were heated at 500 °C during 2 h. For both samples, the diffraction lines (*hkl*): 110, 101, 200, 211, 220, 002, 310, 112, 301, 202 and 321 are present and agree well with the reflections of tetragonal rutile SnO_2 structure (169032-ICSD) which was used as the structural model during the Rietveld refinement. Based on XRPD patterns, no impurity phases are present in both samples. Rietveld refinement showed that the pure SnO_2 sample crystallizes in the tetragonal unit cell with parameters a = 4.741(2) Å and c = 3.194(2) Å, while in the case of Sb-doped SnO_2 sample, a small, but a distinct difference in the unit-cell parameters was observed (a = 4.759(1) Å and c = 3.197(1) Å). Observed increase of the lattice parameters can result from the substitution of Sn^{4+} by larger Sb^{3+} at crystallographic Wyckoff position 2*a* (0,0,0). During the Rietveld refinement, beside the unit-cell parameters, the occupancy parameter of Wyckoff position 4*f*, where oxygen anions is located, has also been refined. Unlike the pure sample having the formula Sn_2O_4, the Sb-doped sample showed the decreased oxygen occupancy. Hence, it can be associated to $Sn_{2-x}Sb_xO_{3.96(1)}$ formulae. Observed decrease in the oxygen content is consistent with the charge balance requirements due to the doping. The incorporation of Sb^{3+} at the position of tetravalent Sn has to be compensated by the decrease of oxygen content in order to preserve the overall neutrality of the compound. The X-ray line broadening analysis was also conducted during the Rietveld refinement on both samples. The average crystallite size decreased with the Sb-doping, from 31(1) nm for pure, un-doped SnO_2 sample, to 19(2) nm for Sb-doped sample. On the other hand, the lattice strain (ε) increased with doping, from 0.09(1) % for pure SnO_2 to 0.21(2) % for Sb-doped sample. Such finding can be explained by the fact that the incorporation of Sb^{3+} is accompanied with the generation of lattice defects in SnO_2. The defects increase the lattice strain, and consequently, slows down the growth of crystallites in the case of doped sample.

Although the difference in crystallite sizes between doped and un-doped sample, calculated from X-ray line broadening analysis, is not so pronounced, the effect of doping on overall morphology is quite obvious for electron

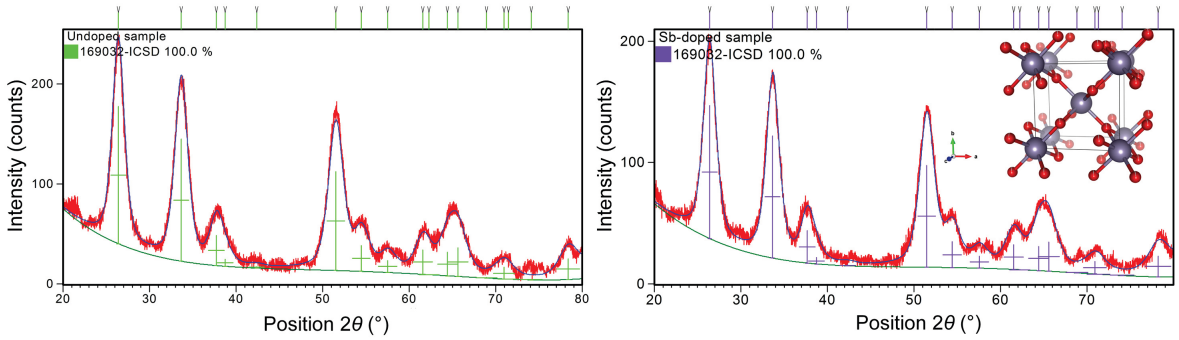

Figure 1. Rietveld refinements for SnO_2 and Sb-doped SnO_2 samples. Experimental patterns are given as red lines while the calculated diffraction patterns are shown by blue lines. Diffraction positions for the SnO_2 and Sb-doped SnO_2 are shown by green and violet vertical marks, respectively. The inset shows Sb-doped SnO_2 structure obtained upon the structure refinement.

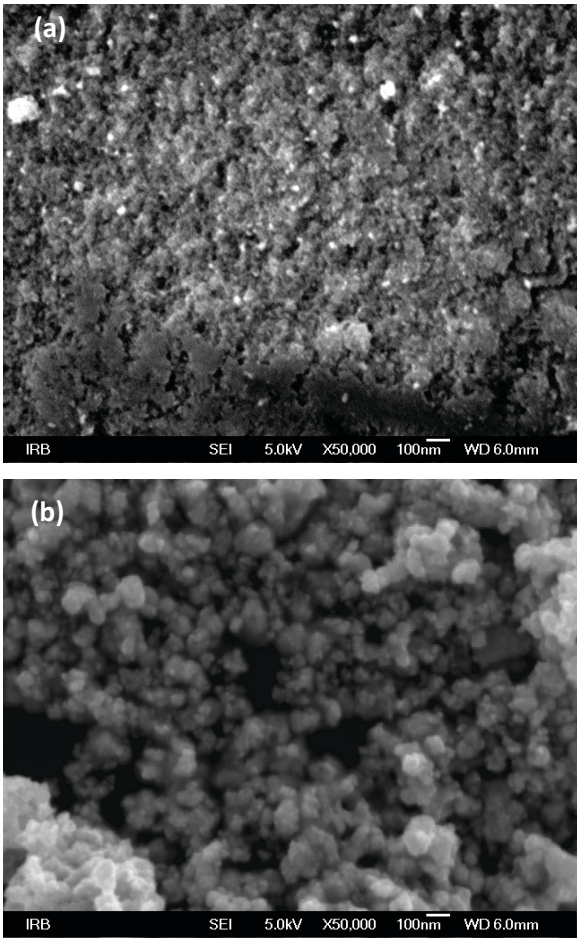

Figure 2. SEM images of: a) SnO_2 and b) Sb-doped SnO_2.

microscopy images shown in Figure 2. The particles of pure SnO_2 sample are assembled very tightly, showing a quite compact morphology (Figure 2a), whereas the SEM image of Sb-doped SnO_2 sample clearly shows the individual particles and some small agglomerates separated with significant number of voids and channels (Figure 2b).

Figure 3 shows the cyclic voltammograms of SnO_2 and Sb-doped SnO_2 deposited onto glassy carbon support. It is evident from the recorded responses that SnO_2 shows high currents in a wide potential range, and no redox peaks are observed. More significant activity of both materials was observed in potential range more negative to 0 V in comparison to the activity in positive potential range. That is in accordance with redox reaction potential characteristic for oxidised tin species.[20] Similar electrochemical performances and similar specific capacitance values were obtained for SnO_2 hollow spheres.[13] These characteristics could provide its application as a negative electrode in supercapacitor. Moreover, it would be a perfect counter-electrode for one of the most *promising* candidates for positive electrode material, *i.e.* MnO_2.[1,21–25]

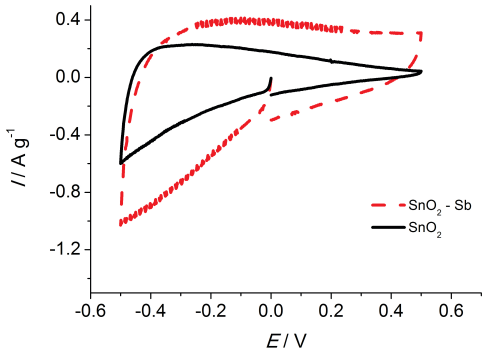

Figure 3. Cyclic voltammograms of SnO_2 and Sb-doped SnO_2 deposited onto glassy carbon support, 50 mV s^{-1}.

In literature, a reaction mechanism of SnO_2 is related to the following reversible process:[16]

$$(SnO_x)_{surface} + C^+ + e^- \rightleftarrows (SnO_x^-C^+)_{surface} \quad (1)$$

that involves surface double layer charging, or:

$$SnO_x + C^+ + e^- \rightleftarrows SnO_x^-C^+ \quad (2)$$

that is followed by intercalation of supporting electrolyte cations, C^+, and / or protons upon reduction and deintercalation upon oxidation. These mechanisms are in accordance with those reported for other metal oxides.[26,27]

From the results obtained in this work, it is evident that ideal capacitive behaviour that includes constant current in wide potential range is not registered.[28] Also, it is apparent that the significant electrochemical activity was registered at the negative potentials . Therefore, to analyse charge storage capacitance, the electrode was cycled at different scan rates in the potential range from 0 V to –0.5 V (Figure 4). More negative potentials were omitted in order to avoid reduction of SnO_2 to metallic tin. The obtained results reveal that tested materials retained similar shape of cyclic voltammetry curve at different scan rates (Figure 3), from 10 to 300 mV s^{-1}, which is necessary condition for supercapacitor application.

To determine the capacitance values of the obtained layer, the integration of the cyclic voltammogram curves was performed, and is specific capacitance, C_s, F g^{-1}, was calculated according to the equation:

$$Cs = \frac{\int_{E_1}^{E_2} IdE}{2vm(E_1 - E_2)} \quad (3)$$

where, I is the current, A, E is the potential, V, m is the mass of active material, g, v is the scan rate, V s^{-1} and E_1 and E_2 are the cycling limits, V.

Capacitive values registered for SnO_2 ranged from 2.36 to 3.67 F g^{-1} while capacitive values for Sb-doped SnO_2 varied from 4.06 to 6.89 F g^{-1} (Table 1). It can be assumed that doping process has increased material conductivity and accordingly utilisation of active material was more effective. Better capacitive response for Sb-doped SnO_2 could also be consequence of higher porosity of material as evident from SEM results (Figure 2) or different crystallite size. Also, cyclic voltammogram presented in Figure 3 indicates that Sb-doped SnO_2 shows more pronounced electrochemical activity at positive potentials, compared to SnO_2, which points to possibility to utilise these materials in a wider potential range.

In this study, the obtained specific capacitances of SnO_2 and Sb doped SnO_2 are similar to the values previously reported by Wu *et al.*[15] However, specific capacitance obtained for amorphous nanostructured SnO_x coating prepared by electrochemical method ranged from 80–240 F g^{-1}.[16] In other investigation, it was reported that electrochemical synthesis resulted in amorphous SnO_2 structure and specific capacitances of 100–270 F g^{-1} at scan rate from 2–200 mV s^{-1}, respectively.[17] Cho *et al.*[29] have prepared tin oxide on ITO support by applying constant current and the obtained material resulted with specific capacitance value of 43 F g^{-1}. Electrochemically prepared SnO_2 was not additionally heat-treated and it can be assumed that the material obtained by this method is more hydrous than our samples. Higher amount of water might be convenient for faster ion exchange and consequently higher specific pseudocapacitance values.

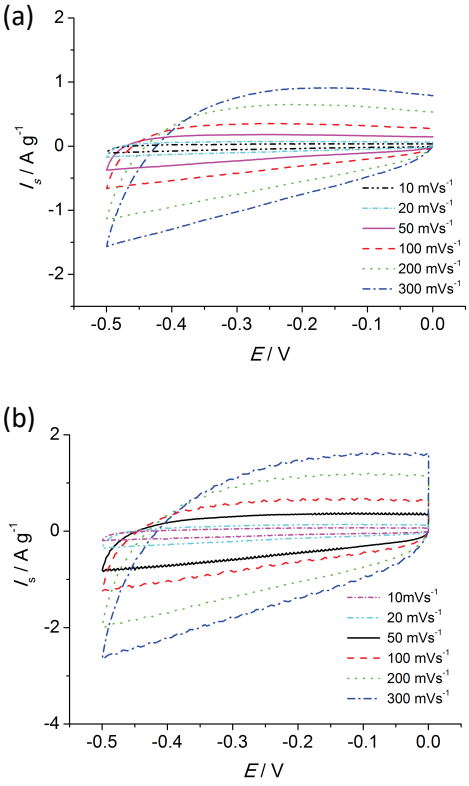

Figure 4. Cyclic voltammograms of (a) the pure SnO_2 and (b) Sb-doped SnO_2, deposited at glassy carbon support at different scan rates.

The amount of water in the pure SnO_2 sample prepared in this work was determined by thermogravimetric analysis (TGA curve is not presented here). It was shown that the sample contains 3 % of physisorbed water and only 4 % of chemisorbed water. Accordingly, although increased conductivity of Sb-SnO_2 has improved specific capacitance and it has shown more significant activity at positive potentials, the obtained values are still much lower in comparison to the values reported for electrochemically prepared SnO_2. The importance of water was previously reported for RuO_2 and MnO_2[30–32] and that was not considered for SnO_2 according to the authors' knowledge.

EQCN measurements were carried out in order to investigate the processes involved in pseudocapacitive redox reaction of SnO_2. For this purpose, SnO_2 and Sb-doped SnO_2 were applied to a platinum electrode of EQCN. As evident from Figure 5a and Figure 5b reduction process is characterised by mass loss while oxidation process is characterised by mass gain. In order to prove that mass change is not a support characteristic (Figure 5c) EQCN experiments were carried out at bare platinum electrode and no mass change was registered. Therefore, mass change can be attributed only to SnO_2 redox reactions. In this work, the observed mass change is not in accordance with previous reports[26] which considered that cation intercalation / deintercalation takes place during SnO_2 reduction /oxidation (reaction(2)).[16] The obtained behaviour could be explained by the fact that SnO_2 redox reaction is not characterised by simple cation intercalation / deintercalation process. This redox reaction rather includes structural changes of the host material similar to those

Table 2. Dependence of specific capacitance C_s (F g^{-1}) with scan rate for the pure SnO_2 and Sb-doped SnO_2.

v / mV s^{-1}	$C_s(SnO_2)$ / F g^{-1}	C_s(Sb-SnO_2) / F g^{-1}
10	3.67	6.85
20	3.67	6.89
50	3.34	5.87
100	3.11	5.90
200	2.68	4.77
300	2.36	4.06

accompanying Li^+ intercalation into SnO_2.[33] Thus, the reaction mechanism proposed in this work is:

$$SnO_x + nH_2O + 2ne^- \rightleftarrows SnO_{x-n} + 2nOH^- \quad (4)$$

This reaction involves water molecules and expulsion of OH^- during SnO_x reduction process and intercalation of oxygen within SnO_{x-1} during oxidation reaction. Therefore, mass loss / gain was registered during reduction / oxidation process, respectively. This suggests that it is important for sample to contain hydrous parts that will enhance oxygen exchange and overall redox reaction. These hydrous parts are expected at boundaries between the crystallites and it should provide percolation paths for OH^- conduction. However, content of water should be controlled in order to provide percolation paths for electron conduction.[32]

The pure SnO_2 prepared herein contains low amount of water (7 %) and this resulted in aggravated OH^- expulsion / oxygen intercalation within the bulk of material and small specific capacitance values. Only the surface of the material that was in contact with water was probably utilised in pseudocapacitive redox reaction. The doping process has increased both specific capacitance value and potential range of activity. However, additional structural modification of SnO_2 is required in order to improve the capacity for charge storage.

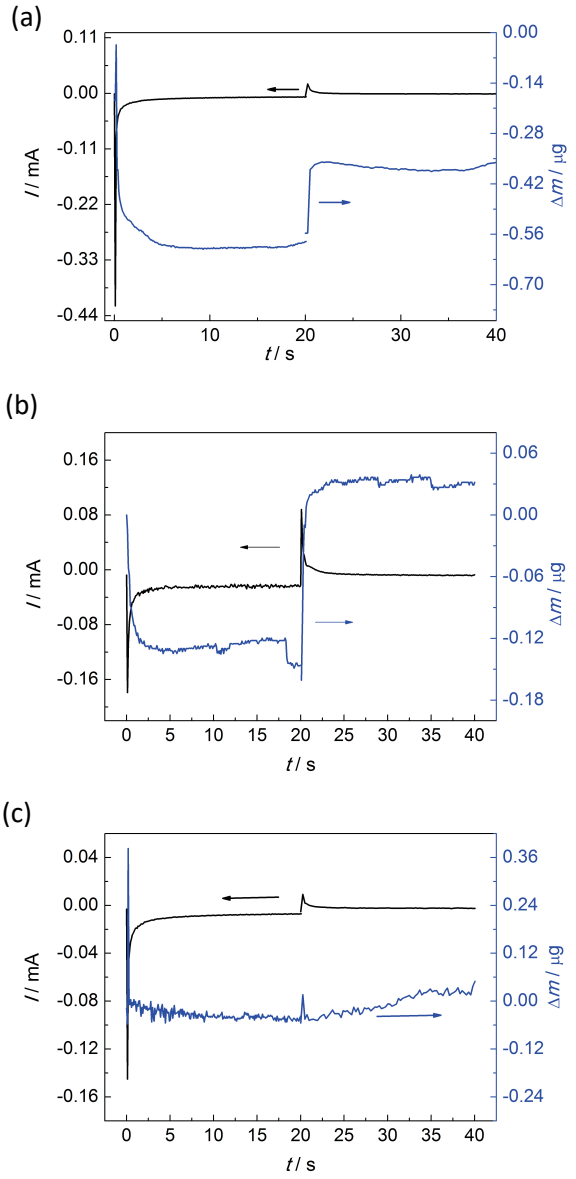

Figure 5. Mass changes and current transients for: (a) SnO_2, (b) Sb-doped SnO_2 and (c) bare platinum electrode after potential steps from 0 to –0.5 V and from –0.5 to 0 V .

CONCLUSION

SnO_2 and Sb-doped SnO_2 were successfully prepared by sol-gel method. The obtained materials showed pseudocapacitive behaviour, since high currents were registered within the potential range of investigation. More pronounced electrochemical activity was obtained at the potentials negative to 0 V *vs.* SCE indicating that SnO_2 is convenient for anode material in supercapacitors application. It was demonstrated that Sb-doping increased specific capacitance values of SnO_2. However, it was shown that water content would also be important for pseudocapacitive properties besides the doping process. EQCN measurements have shown that mass loss / gain was obtained during SnO_2 reduction / oxidation process. The mass change indicates that redox reaction investigated in this work does not include proton / cation exchange process, as it was reported for other metal oxides, but it includes structural changes with oxygen expulsion / intercalation.

REFERENCES

[1] N. Šešelj, D. Sačer, M. Kraljić Roković, *Kem. Ind.* **2016**, *65*, 127.
[2] C. D. Lokhande, D. P. Dubal, O. S. Joo, *Curr. Appl. Phys.* **2011**, *11*, 255.
[3] L. Coustan, A. L. Comte, T. Brousse, F. Favier, *Electrochim. Acta* **2015**, *152*, 520.
[4] I. H. Kim, K. B. Kim, *J. Electrochem. Soc*. **2006**, *153*, A383.
[5] D. Sačer, M. Kralj, S. Sopčić, M. Košević, A. Dekanski, M. Kraljić Roković, *J. Serb. Chem. Soc.* **2017**, *82*, 411.
[6] S. Liu, Y. Liu, W. Song, J. Song, C. Wang, G. Shao, X. Qin, *J. Solid State Electrochem.* **2015**, *19*, 1321.
[7] P. Sun, H. Yi, T. Peng, Y. Jing, R. Wang, H. Wang, X. Wang, *J. Power Sources* **2017**, *341*, 27.

[8] V. Velmurugana, U. Srinivasaraoa, R. Ramachandrana, M. Saranya, *Mater. Res. Bull.* **2016**, *84*, 145.
[9] V. V. Panić, A. B. Dekanski, R. M. Stevanović, *J. Power Sources* **2010**, *195*, 3969.
[10] X. W. Lou, Y. Wang, C. Yuan, J. Y. Lee, L. A. Archer, *Adv. Mater.* **2006**, *18*, 2325.
[11] X. W. Lou, C. M. Li, L. A. Archer, *Adv. Mater.* **2009**, *21*, 2536.
[12] R. Li, X. Ren, F. Zhang,C. Du, J. Liu, *Chem. Commun.* **2012**, *48*, 5010.
[13] S. Ren, Y. Yang, M. Xu, H. Cai, C. Hao, X. Wang, *Colloids Surf. A* **2014**, *444*, 26.
[14] K. Karthikeyan, S. Amaresh, D. Kalpana, R. KalaiSelvan, Y. S. Lee, *J. Phys. Chem. Solids* **2012**, *73*, 363.
[15] S. L. Kuo, N. L. Wu, *Electrochem. Solid State Lett.* **2003**, *6*, A85.
[16] M. Wu, L. Zhang, D. Wang, C. Xiao, S. Zhang, *J.Power Sources* **2008**, *175*, 669.
[17] K. R. Prasad, N. Miura, *Electrochem. Commun.* **2004**, *6*, 849.
[18] R. K. Selvan, I. Perelshtein, N. Perkas, A. Gedanken, *J. Phys. Chem. C* **2008**, *112*, 1825.
[19] S. N. Pusawale, P. R. Deshmukh, C. D. Lokhande, *Appl.Surf.Sci.* **2011**, *257*, 9498.
[20] M. Šeruga, M. Metikoš-Huković, T. Valla, M. Milun, H. Hoffschultz, K. Wandelt, *J. Electroanal. Chem.* **1996**, *407*, 83.
[21] K. C. Ng, S. Zhang, C. Peng, G. Z. Chen, *J. Electrochem. Soc.* **2009**, *156*, A846.
[22] D. Belanger, T. Brousse, J. W. Long, *Electrochem. Soc. Interface* **2008**, *17*, 49.
[23] S. Xiao, F. Bi, L. Zhao, L. Wang, G. Gai, *J. Mater. Sci.* **2017**, *52*, 7744.
[24] Y. Li, B. Guan, A. Maclennan, Y. Hu, D. Li, J. Zhao, Y. Wang, H. Zhang, *Electrochim. Acta* **2017**, *241*, 395.
[25] J. W. Parka, C. M. Parka, *J. Electrochem. Soc.* **2015**, *162*, A2811.
[26] S. Sopčić, Z. Mandić, G. Inzelt, M. Kraljić Roković, E. Meštrović, *J. Power Sources* **2011**, *196*, 4849.
[27] C. A. Beasley, M. B. Sassin,and J. W. Long , *J. Electrochem. Soc*. **2015**, 162, A5060
[28] T. Brousse, D. Bélangere, J. W. Long, *J. Electrochem. Soc*. **2015**, *162*, A5185.
[29] R. S. Mane, J. Chang, D. Ham, B. N. Pawar, T. Ganesh, B. W. Cho, J. K. Lee, S. H. Han, *Curr. Appl. Phys.* **2009**, *9*, 87.
[30] T. Brousse, M. Toupin, R. Dugas, L. Athouel, O. Crosnier, D. Belanger, *J. Electrochem. Soc.* **2006**, *153*, A2171.
[31] G. J. Browning, S. W. Donne, *J. Appl. Electrochem*. **2005**, *35*, 871.
[32] W. Dmowski, T. Egami, K. E. Swider-Lyons, C. T. Love, D. R. Rolison, *J. Phys. Chem. B* **2002**, 106, 12677.
[33] X. W. Lou, Y. Wang, C. Yuan, J. Y. Lee, L. A. Archer, *Adv. Mater.* **2006**, *18*, 2325.